Advanced integrated spectrometer designs for miniaturized optical coherence tomography systems

B. I. Akca*[a], B. Považay[b], L. Chang[a], A. Alex[b], K. Wörhoff[a], R. M. de Ridder[a], W. Drexler[b], and M. Pollnau[a]

[a]Integrated Optical MicroSystems Group, MESA+ Institute for Nanotechnology, University of Twente, Enschede, The Netherlands

[b]Center for Medical Physics and Biomedical Engineering, Medical University of Vienna, Austria.

ABSTRACT

Optical coherence tomography (OCT) has enabled clinical applications that revolutionized *in vivo* medical diagnostics. Nevertheless, its current limitations owing to cost, size, complexity, and the need for accurate alignment must be overcome by radically novel approaches. Exploiting integrated optics, the central components of a spectral-domain OCT (SD-OCT) system can be integrated on a chip. Arrayed-waveguide grating (AWG) spectrometers with their high spectral resolution and compactness are excellent candidates for on-chip SD-OCT systems. However, specific design-related issues of AWG spectrometers limit the performance of on-chip SD-OCT systems. Here we present advanced AWG designs which could overcome the limitations arising from free spectral range, polarization dependency, and curved focal plane of the AWG spectrometers. Using these advanced AWG designs in an SD-OCT system can provide not only better overall performance but also some unique aspects that a commercial system does not have. Additionally, a partially integrated OCT system comprising an AWG spectrometer and an integrated beam splitter, as well as the *in vivo* imaging using this system are demonstrated.

Keywords: Arrayed-waveguide gratings, integrated optics, flat focal field, optical coherence tomography

1. INTRODUCTION

Optical coherence tomography is a well-established optical technique in the medical sciences for acquiring micrometer scale-resolution cross-sectional images of specimen in a non-invasive way[1]. Current state-of-the-art OCT systems operate in the frequency-domain, using either a broad-band light source and a spectrometer, also known as "spectral-domain OCT" (SD-OCT), or a rapidly spectrally tuned laser, known as "swept-source OCT" (SS-OCT)[2]. Both systems contain a variety of fiber and free-space optical components and the imaging quality is sensitive to correct alignment of each individual element. To make OCT widely available these limitations have to be overcome by radically different approaches. Integrated optics can drastically reduce manufacturing costs, increase stability, and enables quasi maintenance-free OCT systems.

For an on-chip SD-OCT system, the principal component i.e. spectrometer needs to be miniaturized. Although integration of a spectrometer on a chip is challenging, arrayed-waveguide gratings[3] (AWGs) present a well-established way towards miniaturization. Combining high resolution and large free spectral range (FSR) in a single AWG is highly desirable for numerous applications, e.g. high-resolution OCT systems; however, it is rather difficult to implement. By cascading several AWGs the limitations on resolution and FSR of an AWG can be overcome[4].

AWG spectrometers are usually of the Rowland mounting type[5] which is a limitation of these spectrometers for on-chip OCT applications in which a continuous output spectrum needs to be imaged directly onto a linear detector array, since the curved image plane of the Rowland mounting would result in additional losses and aberrations at the outer detector channels. Therefore, a flat-focal-field spectrometer would be highly desirable for such applications.

Another important issue is the polarization dependency of AWG spectrometers, which affects the sensitivity roll-off the SD-OCT system. An AWG spectrometer is polarization independent if its array waveguides are polarization independent, which can be achieved by balancing the material and waveguide birefringence[6]. Although this approach requires a highly fabrication-tolerant design, it makes AWGs advantageous over bulky spectrometers. In addition, the cost and size of integrated OCT systems will reduce significantly by using polarization-independent AWGs, thus eliminating the components for polarization control.

Here we present advanced design methods to overcome the limitations arising from FSR, polarization dependency, and curved image plane of AWG spectrometers used in previous approaches[7,8] toward on-chip ST-OCT. An AWG

Optical Coherence Tomography and Coherence Techniques VI, edited by Brett E. Bouma, Rainer A. Leitgeb,
Proc. of OSA Biomedical Optics-SPIE Vol. 8802, 880202 · © OSA-2013 SPIE
CCC code: 1605-7422/13/$18 · doi: 10.1117/12.2032504

spectrometer design with very low polarization dependency and its use in an optical low-coherence reflectometry (OLCR) system is demonstrated. Secondly an alternative way of designing a flat-focal-field AWG using an integrated field-flattening lens is presented. Finally, for solving the FSR limitation we propose a cascaded AWG design by utilizing the cyclic nature of the FSR. Additionally, a partially integrated OCT system comprising an AWG spectrometer and an integrated beam splitter and its *in vivo* imaging performance is demonstrated.

2. NOVEL ARRAYED-WAVEGUIDE-GRATING DESIGNS

2.1 Polarization-independent AWG design

A polarization-dependent AWG images a spectral peak at a given wavelength onto different positions for transverse-electric (TE) and transverse-magnetic (TM) polarizations. For an on-chip SD-OCT system comprising a polarization-dependent AWG, the sensitivity roll-off curve is modulated by a cosine function, which causes signal fading at specific depths for mixed TE and TM polarization[9].

The effect of partial light polarization on sensitivity roll-off was investigated for a TE/TM power ratio of 1. The single-wavelength response of the AWG for partial polarization is given in the inset of Fig. 1a. The AWG was not designed to be polarization independent; consequently, a spectral shift of 0.5 nm was measured between TE and TM polarizations. In Fig. 1a, the red dashed line is the calculated signal beat pattern for partial polarization.

The polarization dependency of AWGs can be eliminated by proper waveguide design. As a proof of concept, a non-birefringent AWG centered at 1300 nm was designed with a resolution of $\delta\lambda$ = 0.4 nm and FSR of 20 nm. A material birefringence of 1.5×10^{-3} and fabrication tolerance of ±1% for width and height and $\pm 10^{-3}$ for core refractive index was used in the waveguide design. Silicon oxynitride (SiON)[10] channel waveguides with a width of 2.2 μm, height of 1 μm, and core refractive index of 1.52 were fabricated. The theoretical polarization-dependent shift was calculated as 5×10^{-6} nm and no significant shift was observed in the transmission measurements for the center and outer channels. No beat effect was observed in the OLCR measurements for partial polarization (TE/TM = 1), as shown in Fig. 1b.

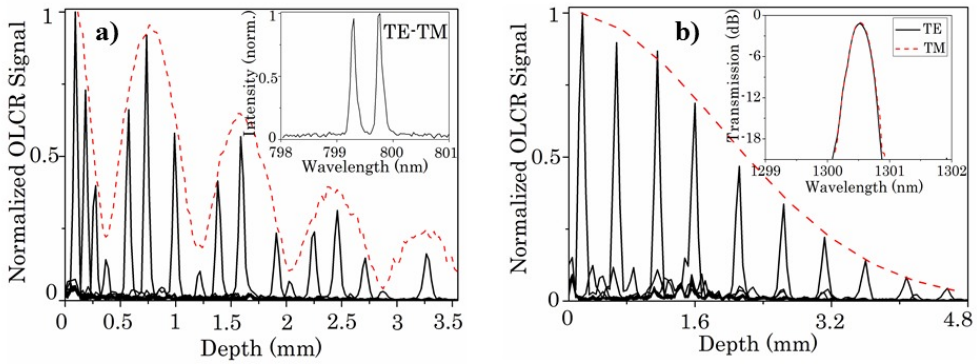

Figure 1. Measured OLCR signal versus depth and calculated roll-off (dashed line) for unpolarized light (TE/TM = 1) of the a) polarization-dependent AWG and b) polarization-independent AWG. The inset in a) is the single-wavelength response of the AWG for TE/TM = 1. The inset in b) is the transmission measurement result of the central channel for TE and TM polarizations. (Figure taken from Ref. 9.)

2.2 Flat-focal-field AWG design

A field-flattening lens is a thin plano-concave negative lens which is placed close to the image plane of an optical system to flatten the curvature of its image surface by minimizing the Petzval aberration[11]. In an AWG, the field curvature induced by the second star coupler can be compensated by placing such a field-flattening lens in the second star coupler. By being close to the image plane it minimally affects the other aberrations. The wavefront of the beam after passing through the lens is not flat, and it diverges for corrected focus[12].

Two AWGs were designed in SiON, one with and one without a field-flattening lens, both having a FSR of 64.8 nm and a resolution of 0.8 nm. The schematic of the field-flattening lens in the second star coupler is shown in Fig. 2a. For the AWG with lens, the refractive index difference between slab and lens region was introduced by applying a 120-nm-thick silicon nitride (Si_3N_4) layer in the lens region (Fig. 2b). The effective refractive indices of slab and lens region were calculated to be 1.50 and 1.61, respectively, which results in a lens radius of R_f = 189 μm.

The performance improvement by the field-flattening lens was demonstrated by comparing the crosstalk, spectral shape, and insertion loss of the two AWGs, as shown in Fig. 2c-e. The adjacent crosstalk was improved by 2 dB and an excess loss value of only 0.4 dB was introduced by the lens. A more pronounced crosstalk improvement for AWGs with higher number of output waveguides is predicted by beam-propagation simulations, as shown in Fig. 2f.

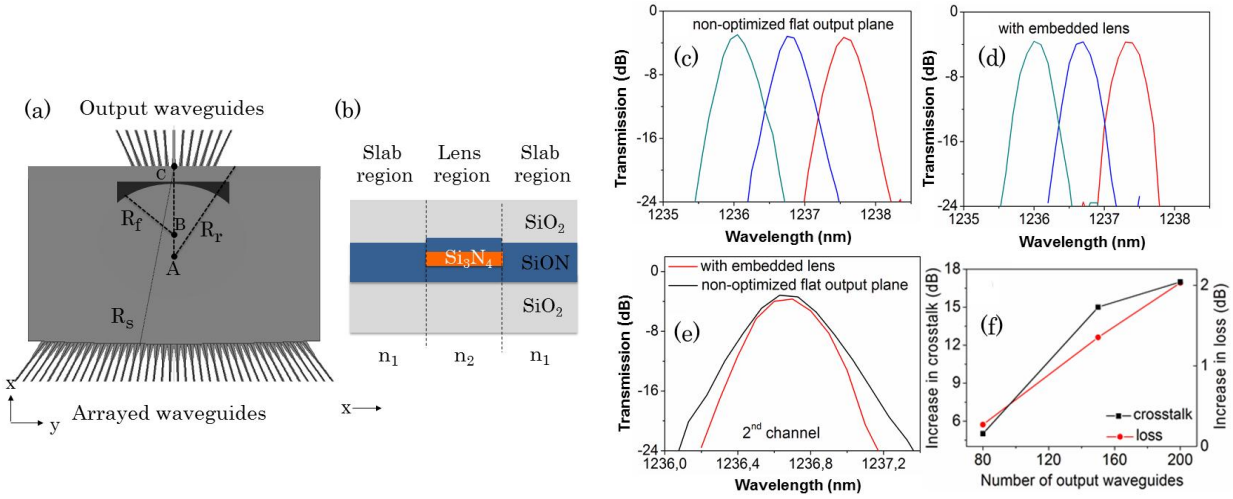

Figure 2. (a) Field-flattening lens in the second star coupler of the AWG. R_r, R_s, and R_f are the radii of curvature of the Rowland circle, the slab region, and the lens, respectively. (b) Cross-section of the star coupler with Si_3N_4 layer. n_1 and n_2 are the effective refractive indices of the slab region with and without Si_3N_4 layer, respectively. Transmission-measurement results for some edge channels of the realized AWGs: (c) with a non-optimized flat output plane, (d) with a field-flattening lens, and (e) comparison of the results given in (c, d) for the 2nd channel. (f) Increase of crosstalk and loss versus number of output channels. (Figure taken from Ref. 12.)

2.3 Cascaded AWG design

An AWG has a cyclic transmission characteristic in that all wavelengths with a spacing equal to the FSR are transmitted simultaneously to a single output waveguide. Here we propose a new cascading technique exploiting the cyclic nature of AWG response, which can provide smaller system size and better overall performance. Instead of the primary AWG having wide flat passbands[13], it could have narrow, closely spaced passbands, equalling the final desired channel spacing. These passbands repeat N times in the desired wavelength range, using the frequency-cyclic nature of the AWG, as illustrated in Fig. 3a. The channel spacing of the secondary AWGs should be equal to the FSR of the primary AWG. In this configuration the FSR of the secondary AWGs defines the FSR of the overall configuration, whereas the channel spacing (resolution) of the primary AWG defines the overall system resolution. In this method, the requirements on resolution and passband flatness of the secondary AWGs are relatively low, as the components in their prefiltered input spectra can be easily separated with very low adjacent-channel crosstalk. Moreover, the complete device size will be much smaller compared to one that is designed with the conventional cascading method, since high-resolution AWGs are generally larger than low-resolution AWGs, so a system with one high-resolution AWG and multiple low-resolution AWGs can be smaller in overall size than one with a low-resolution AWG and multiple high-resolution AWGs. Using this method in OCT systems is more beneficial, since the FSR of an AWG (and, thereby, the wavelength resolution) is constant in frequency, which means that the spectrum is resolved in constant wavenumber Δk intervals, which is appropriate for the OCT signal processing that transforms the spectrum from k to z domain.

Using this method, we designed a cascaded AWG system operating at 800 nm wavelength range with the design parameters given in Table 1. The cascaded AWG system was fabricated using SiON as the core material with a refractive index of 1.5 at 800 nm. The central channel of each secondary AWG was measured in order to investigate the resolution of the final device which is shown in Fig. 3b. We observed a random behavior in terms of channel spacing and positioning of each peak, which we attribute to the non-uniformity of SiON layer thickness and refractive index. Additionally, we observed randomly distributed scattering clusters in the top SiO_2 cladding layer, which could induce effective refractive index fluctuations.

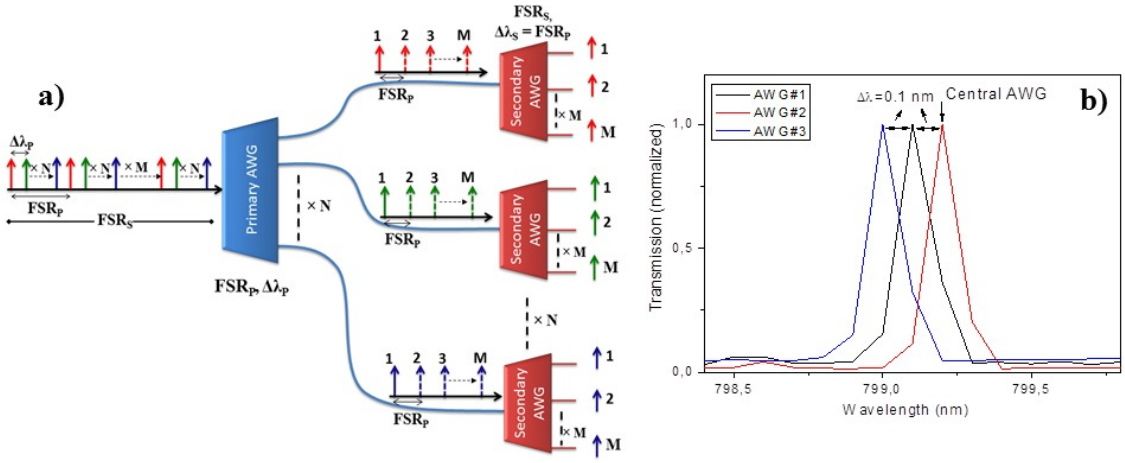

Figure 3. a) Schematic of the cascaded AWG configuration using the cyclic nature of the AWG. FSR_P and FSR_S indicate the FSR of the primary and secondary AWGs, respectively, while $\Delta\lambda_P$ and $\Delta\lambda_S$ are the channel spacings of the primary and secondary AWGs, respectively. $\Delta\lambda_S$ equals FSR_P. The combined system has a FSR equalling FSR_S and a resolution of $\Delta\lambda_P$. b) Measurement results of the central channels of each secondary AWG of the cascaded system using the AWG cyclic nature at 800 nm.

Table 1. Design parameters for the cascaded AWG at 800 nm.

Parameters	Primary AWG	Secondary AWG
FSR (nm)	0.3	30
Channel spacing (δλ, nm)	0.1	0.3
# of output channels	3	100
Device size (cm^2)	1.2×1.3	2.2×1.25

3. PARTIALLY INTEGRATED SD-OCT SYSTEM

A partially integrated SD-OCT system is realized by integrating AWG spectrometer and beam splitter (BS) on a silicon chip[14]. An AWG centered at 1250 nm with a FSR of 136 nm and a wavelength resolution of $\Delta\lambda$ = 0.8 nm forms the integrated spectrometer. The integrated BS is realized by making use of a wavelength-insensitive non-uniform adiabatic coupler[15] with a 3 dB splitting ratio constant over 150 nm wavelength range. *In vivo* performance of the partially integrated SD-OCT system is demonstrated in human skin with an in-tissue maximum depth range of 1.4 mm and an axial resolution of 7.5 µm. Figure 4 shows the *en face* and corresponding cross-sectional tomogram taken from the scar tissue at the index finger of the volunteer. Signal-to-noise ratio (SNR) measured close to the zero delay where both interferometer arms are equal in length was 74 dB at 0.5 mW optical power on the sample, which includes 5 dB fiber-to-chip coupling loss, 7 dB on-chip coupler double-pass excess loss due to imperfect fabrication, and 7.5 dB double-pass transmission loss of the standard microscope objectives. The SNR value could be improved up to the theoretical shot-noise-limited value of 95 dB by reducing these excess losses in the system. The axial resolution and depth range can further improve to <5 µm and <1.4 mm, respectively, by cascading several AWGs at the cost of an increase in device size. In order to compare the imaging performance of the partially integrated SD-OCT system, OCT images of human skin were taken by use of a 1300 nm fiber-based custom-designed SD-OCT system utilizing the same patient interface, source, detection system and processing. The results indicate that the performance of the partially polarized OCT system is comparable to the fiber-based OCT system in terms of axial resolution, however its depth range and sensitivity still need to be improved, although the averaged cross-sections already deliver sufficient quality for delineating biological structures.

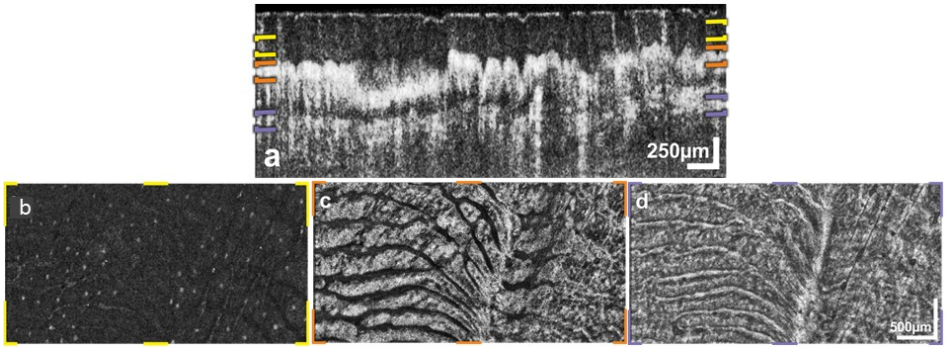

Figure 4. Images of scar tissue at the index finger taken with the partially integrated SD-OCT system: a) Cross section displaying the irregularities caused due to an incision after complete healing. b-d) The *en face* views of different depths. The scale bars denote 250 µm in cross sections and 500 µm in *en face* sections.

4. CONCLUSIONS

In this work we presented advanced AWG designs in order to eliminate specific design-related limitations. A novel flat-focal-field AWG using an integrated field-flattening lens was demonstrated, which could enable one to directly butt-couple them to a detector array, making this design very attractive for applications such as OCT. As a permanent solution to polarization-related signal fading of SD-OCT systems, a polarization-independent AWG was designed and no beat effect was observed in depth ranging measurements for partial polarization. Such a solution would eliminate the need for polarization control with its associated noise and cost penalties in OCT systems. A cascaded AWG design using its cyclic nature was presented, which could increase the imaging range and axial resolution of an OCT system significantly. Finally, *in vivo* imaging with a partially integrated SD-OCT system was demonstrated by acquiring volumetric images of human skin in multiple locations and subjects. In-tissue axial resolution of 7.5 µm and in-tissue depth range of 1.4 mm were achieved. Current performance of the partially integrated OCT system can be further improved to the level of bulky commercial OCT systems with an optimized design and high-quality fabrication facilities.

ACKNOWLEDGEMENTS

This work was financially supported by the Smart Mix Program of the Netherlands Ministry of Economic Affairs and the Netherlands Ministry of Education, Culture and Science, Medical University Vienna, and the European Union projects FUN OCT (FP7 HEALTH, contract no. 201880) and FAMOS (FP7 ICT, contract no. 317744). The authors thank Anton Hollink, Henk van Wolferen, Milorad Jevremovic, Bernhard Rosenauer, and Angelika Unterhuber for technical support, Gabriel Sengo for device fabrication, Dimitri Geskus and XiOPhotonics for angle-polishing the device, Gunay Yurtsever and Alfred Driessen for fruitful discussions, and the Vereniging voor Biofysica en Biomedische Technologie for providing a travel grant.

REFERENCES

[1] Huang, D., Swanson, E. A., Lin, C. P., Schuman, J. S., Stinson, W. G., Chang, W., Hee, M. R., Flotte, T., Gregory, K., Puliafito, C. A., and Fujimoto, J. G., "Optical coherence tomography," Science 254(5035), 1178–1181 (1991).

[2] Fercher, A. F., "Optical coherence tomography – development, principles, applications," Z. Med. Phys. 20(4), 251–276 (2010).

[3] Smit, M. K. and van Dam, C., "PHASAR-based WDM-devices: Principles, design and applications," IEEE J. Sel. Top. Quantum Electron. 2(2), 236–250 (1996).

[4] Takada, K., Yamada, H., and Okamoto, K., "320-channel multiplexer consisting of a 100 GHz-spaced parent AWG and 10 GHz-spaced subsidiary AWGs," Electron. Lett. 35(10), 824–826 (1999).

[5] Rowland, H. A., "On concave gratings for optical purposes," Phil. Mag. 16(5), 197–210 (1883).

[6] Wörhoff, K., Roeloffzen, C. G. H., de Ridder, R. M., Driessen, A., and Lambeck, P. V., **"**Design and application of compact and highly tolerant polarization-independent waveguides**,"** IEEE J. Lightwave Technol. 25(5), 1276–1283 (2007).

[7] Nguyen, V. D., Akca, B. I., Wörhoff, K., de Ridder, R. M., Pollnau, M., van Leeuwen, T. G., and Kalkman, J., "Spectral domain optical coherence tomography imaging with an integrated optics spectrometer," Opt. Lett. 36(7), 1293–1295 (2011).
[8] Akca, B. I., Nguyen, V. D., Kalkman, J., Ismail, N., Sengo, G., Sun, F., Driessen, A., van Leeuwen, T. G., Pollnau, M., Wörhoff, K., and de Ridder, R. M., "Toward spectral-domain optical coherence tomography on a chip," IEEE J. Sel. Top. Quantum Electron. 18(3), 1223–1233 (2012).
[9] Akca, B. I., Chang, L., Sengo, G., Wörhoff, K., de Ridder, R. M., and Pollnau, M., "Polarization-independent enhanced-resolution arrayed-waveguide grating used in spectral-domain optical low-coherence reflectometry," IEEE Photon. Technol. Lett. 24(10), 848–850 (2012).
[10] Wörhoff, K., Klein, E. J., Hussein, M. G., and Driessen, A., "Silicon oxynitride based photonics," Proc. IEEE Intl. Conf. Transparent Optical Networks 3, 266–269 (2008).
[11] Kingslake, R., [Lens Design Fundamentals], Academic Press, Burlington, 297–306 (1978).
[12] Akca, B. I., Sengo, G., Pollnau, M., Wörhoff, K., Driessen, A., and de Ridder, R. M., "Flat-focal-field integrated spectrometer using a field-flattening lens," Opt Lett. 37(20), 4281–4283 (2012).
[13] Akca, B. I., Doerr, C. R., Sengo, G., Wörhoff, K., Pollnau, M., and de Ridder, R. M., "Broad-spectral-range synchronized flat-top arrayed-waveguide grating applied in a 225-channel cascaded spectrometer," Opt. Express 20(16), 18313–18318 (2012).
[14] Akca, B. I., Považay, B., Alex, A., Wörhoff, K., de Ridder, R. M., Drexler, W., and Pollnau, M., "Integration on a microchip — A glimpse into the future of optical coherence tomography," submitted (2013).
[15] Louisell, W. H., "Analysis of the single tapered mode coupler," The Bell Syst. Tech. J. 33, 853–870 (1955).